Communication in Physical Sciences, 2026, 13(9): 1462-1482

Static Reservoir Modelling in the Eastern Niger Delta: Assessing Reservoir Heterogeneity and Uncertainty for Improved Field Development Planning

Philip Asuquo Edem & Selong Unanaonwi Edem

Received: 22 May 2026/Accepted: 21 August 2026/Published: 27 August 2026
https://doi.org/10.4314/cps.v13i9.5

Abstract: *A combined static reservoir modeling study was conducted for three hydrocarbon-bearing sands 1, 2 and 3 of the 'X' Field, eastern Niger Delta, Nigeria. A post-stack, time-migrated 3-D seismic volume of 234 km² with a complete open-hole log suite from three of four wells (KC1–KC4) was provided. Static reservoir modeling was executed in Schlumberger Petrel to integrate the structural, stratigraphic and petrophysical characteristics of the reservoirs and to quantify the hydrocarbon volume in place. The static model was assembled in four connected stages: structural modeling, stratigraphic modeling, lithofacies modeling using sequential indicator simulation (SIS), and petrophysical property modeling using sequential Gaussian simulation (SGS) conditioned to the SIS facies model. A variogram-based, two-point geostatistical approach was adopted, in preference to deterministic kriging or object-based modeling, because it honoured the hard well data exactly, reproduced the natural spatial variability of the reservoir properties away from the wells, and allowed multiple equiprobable realizations to be produced for uncertainty and risk assessment. Thirty-one faults were used as the structural skeleton of the model, with the mapped fault population decreasing from twenty on the depth structure map of Reservoir 1 to nineteen on Reservoir 2 and eight on Reservoir 3. The facies model showed that shale volume decreased with depth, so that Reservoirs 2 and 3 were of better reservoir quality than Reservoir 1. The petrophysical property models returned an effective porosity of 19% to 28% (average 23%), a permeability of 50 mD to 477 mD (averaging 222 mD in Reservoir 1), a hydrocarbon saturation of 56% to 66%, and a net-to-gross of 0.5–3.5 (average 2.0) in Reservoir 1 and 0.5–2.5 (average 1.5) in Reservoir 3. The static model was subsequently used in a Petrel model-dependent volumetric workflow, together with the interpreted oil–water contact, to calculate total oil in place of 6,090 × 10³ bbl, 4,381 × 10³ bbl and 5,658 × 10³ bbl for Reservoirs 1, 2 and 3 respectively. The respective recoverable oil volumes were 2,436 × 10³, 1,752 × 10³ and 2,263 × 10³ bbl. The results confirm that Reservoirs 1 and 3 are more prospective and economically viable than Reservoir 2, and demonstrate that a fully integrated static model, built from properly conditioned structural, facies and property models, is indispensable for reliable reserve estimation in structurally complex Niger Delta reservoirs.*

Keywords: *Static reservoir modeling, heterogeneity, uncertainty. petrophysical property modeling, sequential Gaussian simulation, STOOIP, Niger Delta.*

Philip Asuquo Edem
Department of Geology, University of Calabar, Calabar, Cross River State, Nigeria
Email: philipedem407@gmail.com
https://orcid.org/0009-0007-0509-5079

Selong Unanaonwi Edem
Department of Geology, University of Calabar, Calabar, Cross River State, Nigeria
Email : selonguedem@unical.edu.ng
https://orcid.org/0009-0008-5514-3355

Correspondence Author: philipedem407@gmail.com

1.0 Introduction

The Niger Delta is situated in the Gulf of Guinea at a former triple junction of South Atlantic rifting, with an approximate areal extent of 7,000 km². It is among the largest deltas in the world (Doust & Omatsola, 1990) and is a shale-tectonic province and the most productive hydrocarbon basin in West Africa, with about 37 billion barrels of oil and 180 trillion cubic feet of gas as proven reserves. The dominant role of petroleum in Nigeria's economy has sustained the need for efficient exploration, reservoir characterization and field-development strategies aimed at maximizing hydrocarbon recovery while reducing geological and volumetric uncertainty.. To this effect, 3-Dimensional seismic and well-log data interpretation were employed as indispensable tools to better understand the architectural configuration of the subsurface geology and to construct static models of the reservoirs of interest.

The complex structural framework of the Niger Delta, characterized by growth faults, rollover anticlines, shale diapirism and pronounced lateral and vertical facies variations, can result in significant reservoir compartmentalization and heterogeneity. These geological complexities introduce uncertainty into the prediction of reservoir continuity, connectivity and petrophysical-property distribution, particularly in areas where well control is limited. Static reservoir modelling is an essential component of integrated reservoir characterization and field-development planning because the spatial distribution of structural, stratigraphic and petrophysical properties strongly influences reservoir architecture, connectivity, storage capacity and the subsequent prediction of hydrocarbon volumes. Because subsurface information is derived from relatively sparse well observations and seismic interpretations, reservoir models inevitably contain uncertainty in the representation of faults, stratigraphic surfaces, facies distribution and petrophysical properties. Geostatistical modelling provides a means of representing this spatial variability and generating alternative realizations that can be used to evaluate the impact of geological uncertainty on volumetric estimates and development decisions.

. It involves stages such as stratigraphic modeling, structural modeling, facies modeling and petrophysical modeling (Cosentino, 2003), and the tool used for this modeling permits deterministic and probabilistic hydrocarbon reserves to be estimated. Several studies have demonstrated the usefulness of integrated seismic and well-log interpretation, geostatistical simulation and petrophysical modelling for characterizing Niger Delta reservoirs. However, the approaches adopted and the aspects of reservoir uncertainty addressed vary considerably among fields and depobelts.

Recent Niger Delta studies have investigated several aspects of reservoir characterization, including structural styles and reservoir-quality modelling in the Coastal Swamp Depobelt (Akintokewa *et al*., 2023), integrated seismic-attribute and petrophysical characterization of structurally controlled reservoir sands in the eastern Niger Delta (Etukudo *et al*., 2026; Edem *et al*., 2026), and the integration of well-log and three-dimensional seismic data for offshore reservoir description (Akinlabi & Abiodun, 2024). Other studies have examined reservoir heterogeneity and boundary delineation (Sonny *et al*., 2024), while Fajana, *et al.* (2025) demonstrated the application of sequential indicator simulation and sequential Gaussian simulation to quantitative petrophysical and volumetric evaluation. Fajana (2020) further showed the potential of combining geostatistics with artificial neural networks to reduce uncertainty associated with lateral heterogeneity, whereas Fajana (2023) highlighted the spatial dependence of reservoir-characterization uncertainty on the availability and distribution of well control.

(Akintokewa *et al*., 2023).

Despite these advances, an important gap remains in the integrated assessment of reservoir heterogeneity and uncertainty within a unified static-earth modelling framework for structurally complex fields of the eastern Niger Delta. Many previous studies have focused on individual components of reservoir characterization, such as structural interpretation, petrophysical evaluation, seismic-attribute analysis or property modelling, while relatively limited attention has been given to the combined influence of structural architecture, facies variability and spatially distributed petrophysical properties on volumetric uncertainty and field-development planning. Furthermore, uncertainty associated with the distribution of reservoir properties away from the available well control requires explicit consideration through multiple geostatistical realizations rather than reliance on a single deterministic representation.

To address this gap, the present study develops an integrated static reservoir model for the study field by combining structural, stratigraphic, lithofacies and petrophysical-property modelling within a common three-dimensional geological framework. The modelling workflow incorporates sequential indicator simulation for facies distribution and sequential Gaussian simulation for the spatial distribution of reservoir properties, thereby providing multiple geological realizations for evaluating reservoir heterogeneity and uncertainty.

The study integrates three-dimensional seismic data and well-log information to characterize the structural framework, stratigraphic architecture and petrophysical properties of the reservoirs. The integration of these datasets provides a consistent geological framework within which reservoir facies and properties can be spatially distributed, allowing the effects of heterogeneity and uncertainty on hydrocarbon volumetrics to be evaluated.

The resulting static model is expected to provide a more robust representation of reservoir architecture and property variability than interpretations based solely on individual wells or deterministic property distributions. By quantifying the spatial variability of key reservoir properties and its implications for hydrocarbon volumes, the study provides geological information that can support volumetric assessment, uncertainty reduction, reservoir management and field-development planning. The model also provides a geological foundation for subsequent dynamic simulation, production forecasting and evaluation of alternative development strategies.

The aim of this study is to develop an integrated static reservoir model of the study field using three-dimensional seismic and well-log data, with emphasis on characterizing reservoir heterogeneity and quantifying geological uncertainty. Specifically, the study seeks to establish the structural and stratigraphic framework, model lithofacies and key petrophysical properties, evaluate their spatial variability, and use the resulting geological model to estimate hydrocarbon volumes and assess the implications for field-development planning.

The study therefore contributes an integrated and uncertainty-aware geological framework for improved understanding of reservoir heterogeneity and more reliable hydrocarbon volumetric assessment in structurally complex Niger Delta reservoirs.

1.1 Geologic Setting

The Niger Delta is located in the Gulf of Guinea and is regarded as one of the most prolific hydrocarbon provinces in the world. It is typically a wave- and tide-dominated delta located on the Atlantic coast of Africa and fed by the Niger River (Doust & Omatsola, 1990). It is characterized by a thick succession of deltaic sediments that have prograded over the passive margin and overlie a ductile substrate of overpressured shale, reaching a maximum thickness of 10–12 km (Doust & Omatsola, 1990). It is also characterized by large regional and counter-regional extensional growth faults that formed mainly on the delta top, together with a belt of imbricate thrusts and folds at the delta toe. The delta-top growth-fault systems are generally accepted to have formed because of differential progradation and loading of the ductile substrate of over pressured pro-delta shale, and the extensional growth faults are mechanically linked to the contractional fold/thrust system at the delta toe.

The area of study lies within the eastern part of the Niger Delta of the Coastal Swamp Depobelt, with an areal extent of approximately 234 km². Three basic lithostratigraphic subdivisions are typical of the Niger Delta (Evamy *et al*., 1978; Emujakporue & Ngwueke, 2013). The Benin, Agbada and Akata Formations, with the Agbada formation constituting the major producing reservoirs in which hydrocarbons are entrapped by rollover anticlines associated with growth faults (Doust & Omatsola, 1989), and the Akata Formation, about 21,000 ft thick. The reservoirs modeled in this study occur within the Agbada Formation.

2.0 Materials and Methods

The dataset used in this study was provided by an oil company and comprised a post-stack, time-migrated three-dimensional (3-D) seismic volume covering approximately 234 km², together with wireline-log, checkshot and well-deviation data from four wells (KC1–KC4). All seismic interpretation, well-log analysis and static reservoir modelling were performed using Schlumberger Petrel. Complete and usable open-hole log suites were available for wells KC1–KC3, whereas well KC4 contained only checkshot information and was therefore used to support the regional time–depth conversion and seismic-to-well calibration.

2.1 Petrophysical evaluation

Volume of shale (Vsh) was computed from the gamma-ray log following the linear index method, and for the tertiary reservoirs of the study area the Larionov (1969) equation for younger rocks was subsequently applied. Effective porosity was estimated from the corrected neutron and density logs following the procedures described by Hartmann and Beaumont (1999) as well as Asquith & Krygowski (2004). Water saturation was calculated using the Archie (1942) equation for clean sand, and the Indonesian equation of Poupon & Leveaux (1971) and the modified Simandoux (1963) equation for shaly sand, with a cementation exponent of 2.01, a saturation exponent of 2 and a tortuosity factor of 1. The selection of the shaly-sand saturation models was guided by their reported applicability to dispersed-clay reservoirs and by their use in comparable Niger Delta studies. The saturation model applied to each reservoir interval was selected according to the interpreted shale content and lithological character of the interval. Archie's equation was applied to clean-sand intervals, whereas the Indonesian and modified Simandoux formulations were evaluated for shaly-sand intervals. The selected formulation was retained based on its consistency with the interpreted clay content and the available well-log response.

Fajana *et al*. (2021) compared algorithms of Waxman–Smith against Archie-family models in shaly-sand reservoirs of the Pennay Field and found the Archie-derived approaches, of which the Simandoux and Indonesian equations are shaly-sand variants, remained appropriate where clay distribution is dispersed rather than laminated, as was assumed here. Permeability was independently estimated using the Wyllie & Rose (1950), Coates and Denoo (1981), and Owolabi *et al*. (1994) empirical relationships. The resulting estimates were compared, and the relationship providing the most consistent permeability distribution with the interpreted reservoir characteristics was selected for subsequent modelling

2.2 Structural interpretation

Seismic-to-well tie was carried out using the post-stack migrated 3-D seismic volume, checkshot data from well KC3 and mapped well tops, using a Ricker wavelet of 128 ms length at a sampling rate of 2 ms. Faults were mapped on the interpretation window at intervals of 10 traces on the basis of recognizable fault throw, irregular reflector terminations and amplitude alteration in the fault zones. Amplitude gain was applied to enhance reflection continuity, followed by structural smoothing. A variance-edge attribute was subsequently computed to enhance discontinuities associated with fault planes. Faults were mapped on inlines, with the major faults additionally mapped on crosslines. Thirty-one faults (F1–F31) were identified and mapped in this manner. Horizons bounding the reservoirs of interest were mapped in both the inline and crossline directions at intervals of 10 slices (500 m on the ground surface), and the mapped surfaces were converted from time to depth using a linear velocity function (look-up table) generated from a depth-versus-time plot. The interpreted oil–water contact (OWC) was identified primarily from the pronounced resistivity response and its consistency with the gamma-ray, density and neutron-log characteristics across the relevant intervals

2.3 Static reservoir modeling workflow

Static reservoir modeling was carried out in Petrel to produce an integrated structural and petrophysical model of the identified reservoirs, comprising the fault, facies, net-to-gross, porosity, permeability and water-saturation models. The workflow proceeded through four linked stages — structural modeling, stratigraphic modeling, lithofacies modeling and petrophysical property modeling. The discrete facies model and the continuous petrophysical property models were not generated by deterministic interpolation; rather, they were generated stochastically, using sequential indicator simulation (SIS) for facies and sequential Gaussian simulation (SGS), conditioned to the resulting facies model, for the continuous properties. This variogram-based, two-point geostatistical approach was selected as the mathematical basis of the static model because it honored the well data exactly at the well locations, reproduced the natural spatial variability of the reservoir properties away from the wells rather than an over-smoothed average, and permitted multiple equiprobable realizations of the reservoir to be generated for subsequent uncertainty and risk analysis; the underlying formulation is set out in Section 3.4.5.

2.3.1 Structural modeling

Structural modeling is the reconstruction of the geometrical and structural properties of the reservoir and consists of four steps — fault modeling, zonation, pillar gridding and contact mapping — carried out to produce a single data model. Fault polygons created from the faults mapped across the seismic volume served as the input parameters for this stage. A listric pillar type was used for fault modeling, since most of the faults in the study area are listric in nature; each fault was modeled in turn using an increment of 10 m. The thirty-one modeled faults were displayed in a 2-D window, in which an external grid-boundary segment tool was used to connect the edge of one fault to the next, producing a boundary around the hydrocarbon-potential area. Pillar gridding was then used to generate the three-dimensional structural skeleton of the reservoir, comprising top, mid and base skeletons, and to provide the geometric framework for subsequent facies and petrophysical-property modelling. The zonation process defined the resolution of the grid by generating zones within the reservoir, while layering created equal layer thicknesses from the top to the base of each reservoir. Finally, contact mapping was used to define the fluid contacts in the reservoir using the gamma ray, resistivity, neutron and density logs.

2.3.2 Stratigraphic modeling

Stratigraphic modeling incorporated the well-to-well correlation and the integration of the density, neutron, and resistivity, gamma-ray logs to delineate the stratigraphic horizons bounding the major geological sequences within the hydrocarbon-bearing formation, and to display the thickness of each identified reservoir. Stratigraphic modelling was performed to establish the vertical and lateral continuity of the reservoir units and to preserve the interpreted depositional architecture within the three-dimensional grid. Well-to-well correlation was based on the integrated interpretation of gamma-ray, density, neutron and resistivity logs, together with the interpreted seismic horizons and well tops. The correlated reservoir tops and bases were used to define the model zones and layering scheme, thereby providing the stratigraphic framework for subsequent facies and petrophysical-property simulation.

2.3.3 Lithofacies modeling

Lithofacies modeling is important because the environment of deposition is a discrete property that, if wrongly incorporated, has an adverse effect on the distributed properties and, consequently, on the reserve estimate. Two basic lithofacies sand and shale were identified and used for the model. The facies log generated in Petrel was scaled up onto the grid cells using a blocking process, and facies were then simulated across each reservoir unit using the sequential indicator simulation (SIS) method. The major and minor directional ranges of each reservoir were used to define the anisotropy parameters for the variogram models.

2.3.4 Petrophysical property modeling

Petrophysical property modeling assigns petrophysical property values to each cell of the grid. The permeability log generated from the well-log analysis served as the basis for the permeability model, using minimum and maximum scales of 0.1 mD and 10,000 mD; the facies logs were upscaled using an arithmetic averaging method, and the Gaussian simulation method was used to distribute permeability across the model, conditioned to the facies of the modeled zone. The generated porosity logs, with cut-off values adjusted to a minimum of 0 and a maximum of 0.50, were similarly upscaled using arithmetic averaging and conditioned to facies across the model. The net-to-gross log was scaled to a minimum and maximum of 0 and 1, respectively, upscaled, and distributed stochastically across the model. Water saturation was distributed uniformly within the hydrocarbon zones, with minimum and maximum values of 0 and 1. Sequential Gaussian simulation (SGS) was the principal stochastic method used to distribute the porosity, permeability and hydrocarbon-saturation properties across the grid, honoring the underlying facies model.

2.3.5 Stochastic simulation

The lithofacies and petrophysical property models described above were not distributed by simple deterministic interpolation; rather, sequential indicator simulation (SIS) was used to distribute the discrete facies (sand/shale), and sequential Gaussian simulation (SGS), conditioned to the resulting facies model, was used to distribute the continuous petrophysical properties (net-to-gross, effective porosity, permeability and water/hydrocarbon saturation) across the grid. This combined SIS–SGS approach was adopted, rather than a purely deterministic kriging estimate or an object-based approach, because it honored the hard well data exactly at the well locations, reproduced the spatial variability of the reservoir properties away from the wells, and permitted multiple equiprobable realizations of the reservoir to be generated for subsequent uncertainty and risk analysis. This same combination of algorithms has been applied in other recent field studies; Al-Mudhafar *et al*. (2024) used SISIM for facies and SGSIM for porosity and permeability in a heterogeneous clastic reservoir in Iraq to support history matching, and Rezaei *et al*. (2023) likewise used variogram-based, seismic-conditioned pluri-Gaussian facies simulation to model a heterogeneous carbonate reservoir in southwestern Iran. Within the Niger Delta specifically, Fajana (2025) coupled the same class of two-point geostatistics with an artificial-neural-network property predictor to reduce lateral-heterogeneity uncertainty in the static model of the 'P' Field, an approach that is complementary to, though methodologically distinct from, the purely variogram-based SIS–SGS formulation retained in the present study for its direct honoring of hard well data and its capacity to generate multiple equiprobable realizations.

The spatial continuity of each variable was first quantified using an experimental semi-variogram, computed from the upscaled well-log data and modeled with a spherical or exponential variogram model of the form:

$$\gamma(h) = \frac{1}{2} \times E\left\{\left(Z(x+h)\right)^2\right\} \qquad (1)$$

where γ(h) is the semi-variance at lag distance h, Z(x) is the value of the regionalized variable (facies indicator or petrophysical property) at location x, and Z(x + h) is its value at a point separated from x by the lag vector h. The variogram model, together with its range, sill and nugget, was used to derive the kriging weights applied at each simulation node.

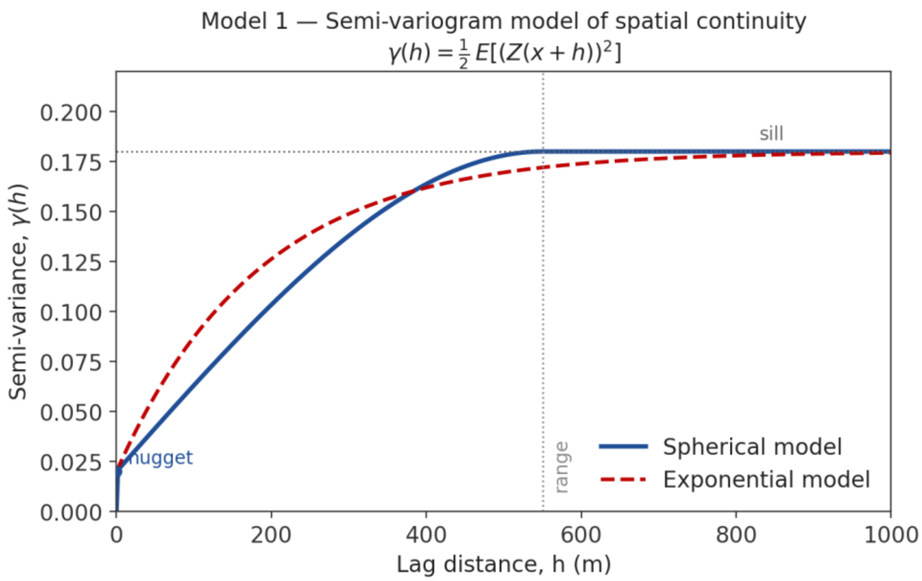

Fig. 1. Spherical and exponential semi-variogram models of γ(h) plotted against lag distance h, showing the nugget, sill and range used to derive the kriging weights applied at each simulation node

For facies simulation, the sand/shale lithofacies was first coded as a binary indicator variable, i(x; k), equal to 1 if facies k was present at location x and 0 otherwise. At each unsampled grid node x_0, the local probability of occurrence of facies k was estimated by simple kriging of the indicator data:

$$i^*(x_0;\ k) = \Sigma\ \lambda_i(x_0) \times i(x_i;\ k) \qquad (2)$$

where $i^*(x_0;\ k)$ is the estimated (kriged) probability that facies k occurs at node x_0, $i(x_i;\ k)$ is the indicator value at the i-th conditioning datum, and $\lambda_i(x_0)$ are the kriging weights gotten by solving the indicator-variogram system for that node. A facies was then drawn at random from the resulting local probability distribution, node by node, along a random path across the grid, with each newly simulated value added to the conditioning data set used for all subsequent nodes; this sequential procedure was repeated until every cell of the 3-D grid had been assigned a facies.

For the continuous petrophysical properties, the upscaled well-log values were first transformed to a standard normal (Gaussian) distribution using a normal-score transform. At each grid node x_0, simple kriging was used to estimate the local conditional mean, $Z^*_{sk}(x_0)$, and kriging variance, $\sigma_{sk}(x_0)$, of the transformed variable, honoring only the data (and previously simulated values) falling within the facies domain established by the SIS model at that node. A simulated value was then drawn as:

$$Z(x_0) = Z^*_{sk}(x_0) + \sigma_{sk}(x_0) \times G\,(0,1) \qquad (3)$$

where $Z^*_{sk}(x_0)$ is the simple-kriging estimate of the conditional mean at node x_0, $\sigma_{sk}(x_0)$ is the simple-kriging standard deviation at that node, and $G(0,1)$ is a value drawn at random from a standard normal distribution.

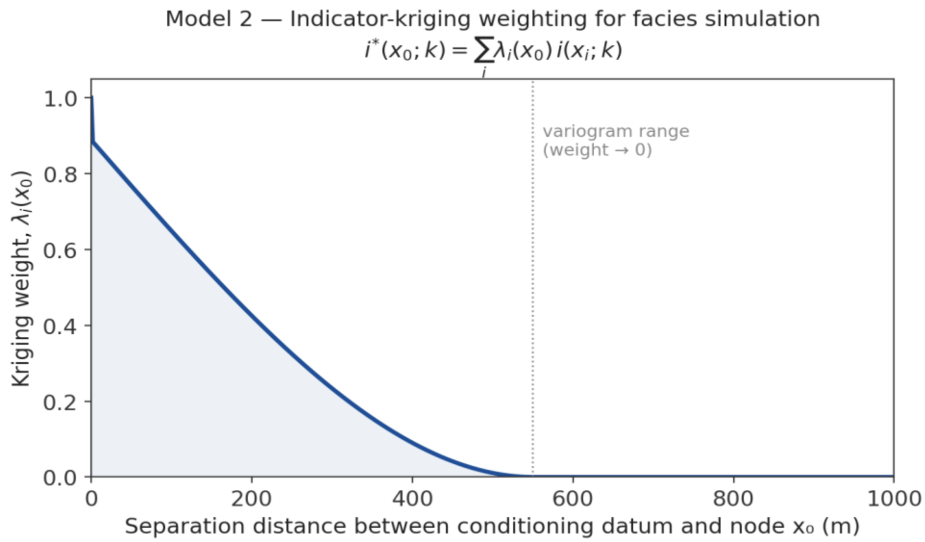

Fig. 2. Indicator-kriging weight $\lambda_i(x_0)$ assigned to a conditioning datum, plotted against its separation distance from the estimation node x_0. The weight is close to 1 at zero separation and declines to zero beyond the variogram range, consistent with the semi-variogram model of Fig. 1

As with the facies simulation, this was performed sequentially along a random path, with each newly simulated value retained as an additional conditioning datum for the nodes visited thereafter, and the simulated values were finally back-transformed from the normal-score space to the original units of net-to-gross, porosity, permeability and saturation. Conditioning the petrophysical simulation to the facies model in this manner ensured that the simulated porosity, permeability and saturation populations differed appropriately between the sand and shale facies, rather than being averaged into a single unrealistic field-wide trend.

Reserve estimation is an integral and essential aspect of the static (geologic) model, as it forms the basis on which exploration and development decisions are made. The structural and property models of individual reservoir and the interpreted oil–water contact were used as the major inputs to the Petrel model workflow to calculate the stock tank oil originally in place (STOOIP).

2.3.7 Model validation and uncertainty assessment

Model validation was performed by comparing the statistical distributions of the simulated properties with those of the upscaled well data. The mean, standard deviation, minimum and maximum values, as well as the cumulative distribution functions of porosity, permeability, net-to-gross and saturation, were compared between the conditioning data and the simulated realizations. The reproduced spatial continuity was evaluated by comparing experimental variograms of the simulated models with the corresponding input variogram models. Multiple equiprobable realizations were generated to assess the uncertainty associated with the spatial distribution of reservoir properties and the resulting hydrocarbon volumes.

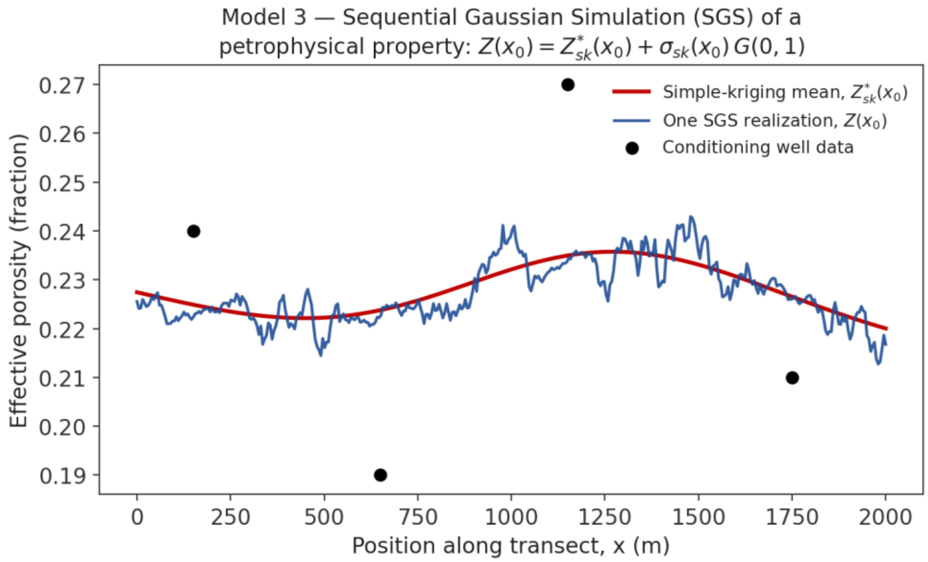

Fig. 3. Sequential Gaussian Simulation (SGS) of a petrophysical property: $Z(x_0) = Z'_{sk}(x_0) + \sigma_{sk}(x_0) \times G(0,1)$; the fluctuating line is one simulated realization, showing greater variability away from the wells where the kriging standard deviation is larger

2.3. 6 Volumetric estimation

3.0 Results and Discussion

3.1 Geosatistical basis of the modeled results

The spatial distributions obtained from the static model reflect the continuity and variability captured by the fitted variogram models and the conditioning well data. The SIS–SGS workflow preserved the observed facies and petrophysical-property characteristics at the well locations while allowing their spatial variability to be represented between wells. Consequently, the resulting models exhibit heterogeneous distributions of facies, net-to-gross, porosity, permeability and hydrocarbon saturation rather than the spatial smoothing expected from a purely deterministic interpolation approach.

The degree of spatial variability away from the wells is controlled by the variogram range and the associated kriging uncertainty. Areas close to well control are therefore more strongly constrained by observed data, whereas areas farther from the wells have greater uncertainty in the predicted property distributions. This distinction is important for interpreting the reservoir-quality maps and for assessing the reliability of the subsequent volumetric estimates.

The semi-variogram model of Equation 1, fitted to the upscaled well-log data for each facies indicator and petrophysical property. This controlled the range over which the reservoir properties were treated as spatially correlated. Grid nodes within the variogram range of a well were consequently estimated with a kriging weight, $\lambda_i(x_0)$, close to unity (Equation 2), causing the simulated facies and property values to honour the well data almost exactly in the immediate vicinity of the wells. Nodes beyond the range were estimated increasingly from the global statistics of the data set; so that reservoir heterogeneity away from the wells is a modeled, rather than an interpolated, feature of the resulting maps.

This mathematical basis explains several features of the results presented in Sections 4.3–4.7. Because the sequential Gaussian simulation of Equation 3 draws each simulated value from a local Gaussian distribution centered on the simple-kriging mean, with a spread proportional to the simple-kriging standard deviation, the net-to-gross, porosity, permeability and hydrocarbon-saturation models retain a level of small-scale spatial variability, rather than the smoothly interpolated surfaces that a purely deterministic method would produce, and this variability is visibly greater in areas farther from well control, where the kriging standard deviation is largest. Conditioning the property simulations to the facies model generated by sequential indicator simulation, in turn, ensured that the simulated porosity, permeability and saturation populations differed appropriately between the sand and shale facies domains, rather than being averaged into a single, geologically unrealistic field-wide trend; the resulting facies-dependent contrast in petrophysical quality, most evident in the systematic decrease in shale volume, and corresponding improvement in net-to-gross and porosity, with depth (Section 4.3), is therefore as much a product of the SIS–SGS mathematical formulation as it is of the underlying geology. As Fajana (2023) has noted in a review of reservoir-characterization uncertainty as a function of spatial location, this distance-dependent behavior of the kriging variance is not incidental to the method but is its central practical value, since it gives an explicit, quantitative basis for distinguishing well-constrained volumes from those that are extrapolated; a distinction returned to for the STOIIP Figures of this study in Section 4.10.

3.2 Structural model

The structural model was built using the results of the fault model of the identified reservoirs. The reservoirs were highly faulted, and the number of faults decreased with increasing depth in the field: twenty faults were recognized on the depth structure map of Reservoir 1, nineteen on Reservoir 2, and eight on Reservoir 3 (Table 2). This significant decrease in fault population with depth indicates that not all faults were significant in the deeper horizons. Fault F2, for example, affected only Reservoir 1. The major bounding faults trend in the northeast–southwest direction and divide the field into a northern footwall block and a southern hanging-wall block, which align with the regional listric growth-fault architecture of the Niger Delta. This fault density is considerably higher than that reported for other recently modeled Niger Delta fields Alakuko and Falowo (2023), for example, mapped only eight crestal and synthetic faults across the three reservoir sands of the offshore KUKO Field. The relatively high fault count reflects the structurally complex nature of the study field and indicates that faulting may exert an important control on reservoir compartmentalization and connectivity, and that the resulting compartmentalization has a material bearing on the volumetric estimates presented in Section 4.9.

Although 47 fault intersections (Table 1) were identified across the three reservoir horizons, these corresponded to 31 unique faults in the three-dimensional structural framework, with individual faults terminating or becoming insignificant at different stratigraphic levels.

The observed decrease in fault occurrence from Reservoir 1 to Reservoir 3 suggests that the structural influence of the interpreted fault system varies vertically within the stratigraphic succession. The greater fault density in Reservoir 1 may result in stronger compartmentalization and potentially more complex fluid communication, whereas the fewer faults affecting Reservoir 3 may indicate comparatively simpler structural connectivity. However, the sealing or transmissibility behaviour of individual faults cannot be established from geometry alone and would require additional evidence such as juxtaposition analysis, shale-gouge assessment or dynamic pressure data.

The facies model was built on the environment of deposition, with sand and shale used as the two basic lithofacies. The facies were scaled up using a blocking process, and the resulting model was used to ascertain the petrophysical properties of the identified reservoirs

Table 1: Number of faults mapped on the depth structure map of each reservoir top

Reservoir top	Number of faults mapped
Reservoir 1	20
Reservoir 2	19
Reservoir 3	8

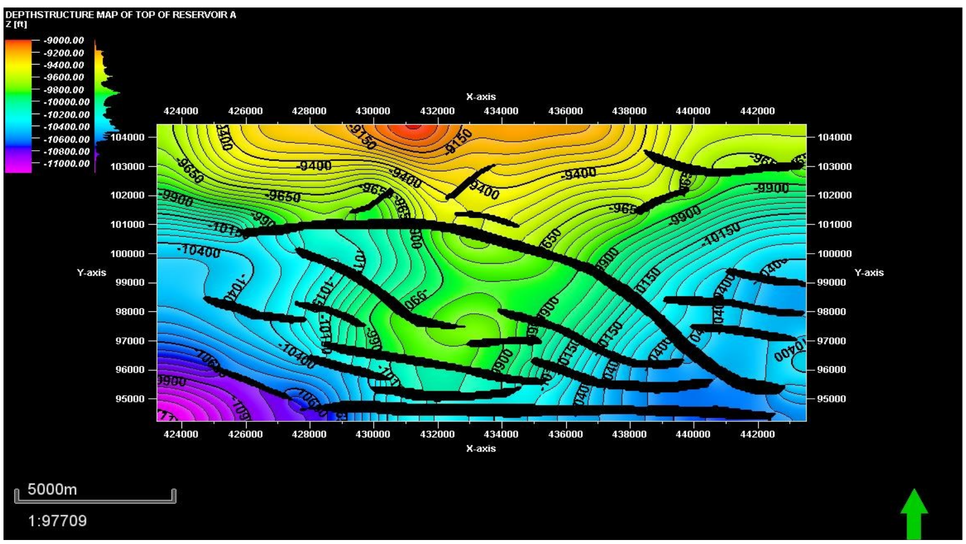

Fig. 2: Structural contour map of the top of Reservoir 1, with twenty faults

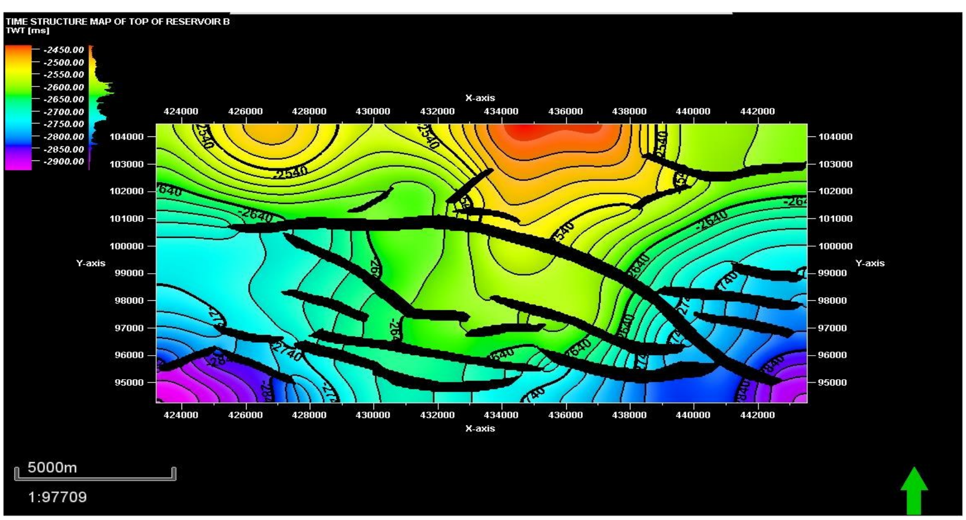

Fig. 3: Structural contour map of the top of Reservoir 2, with nineteen faults.

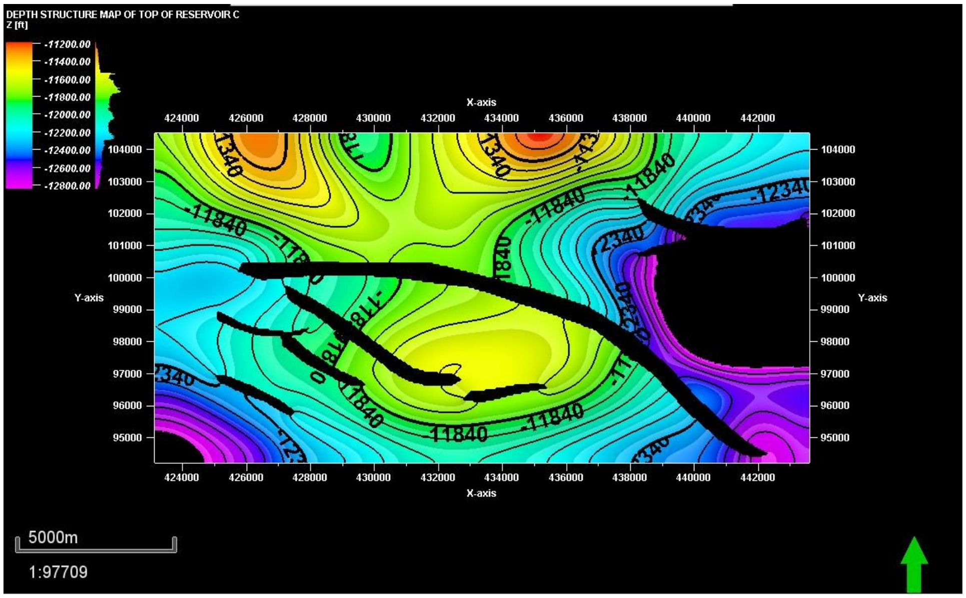

Fig. 4: Structural contour map of the top of Reservoir 3, with eight faults

4.3 Facies model

. The model reveals that, within the three reservoirs, the volume of shale decreases with depth, with Reservoir 1 containing a greater volume of shale than Reservoirs 2 and 3, implying that The lower shale content observed in Reservoirs 2 and 3 suggests a greater proportion of reservoir-quality sand than in Reservoir 1. This interpretation is further evaluated using the net-to-gross, porosity and permeability modelsThis depth-dependent facies pattern is precisely what the sequential indicator simulation of Equation 2 is designed to reproduce: the indicator-kriging weights decay with distance from each well, so the simulated sand/shale proportions honor the well-observed decrease in shale volume with depth exactly at the wells while extrapolating it, via the fitted variogram, into the inter-well area.

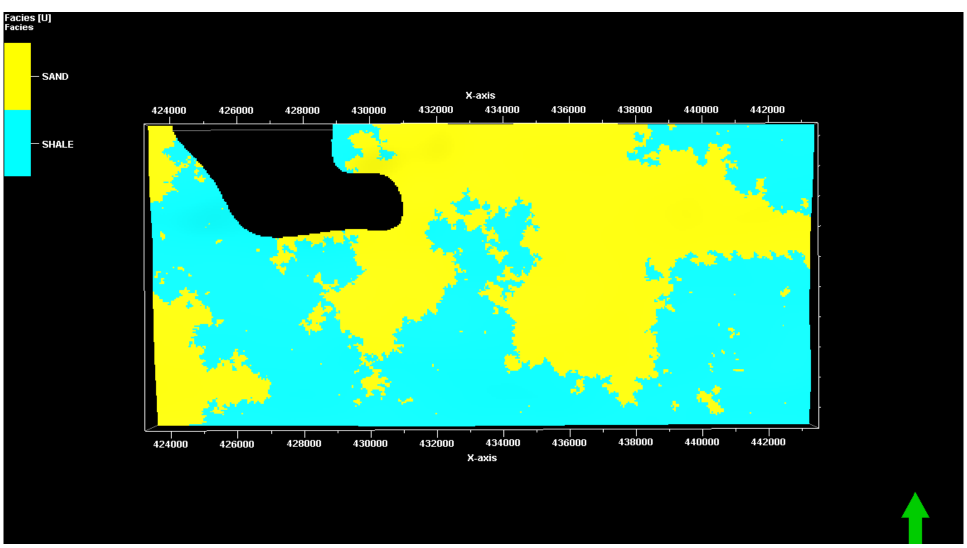

Fig. 5. Facies model of Reservoir 1, showing the distribution of sand (reservoir) and shale (non-reservoir) facies.

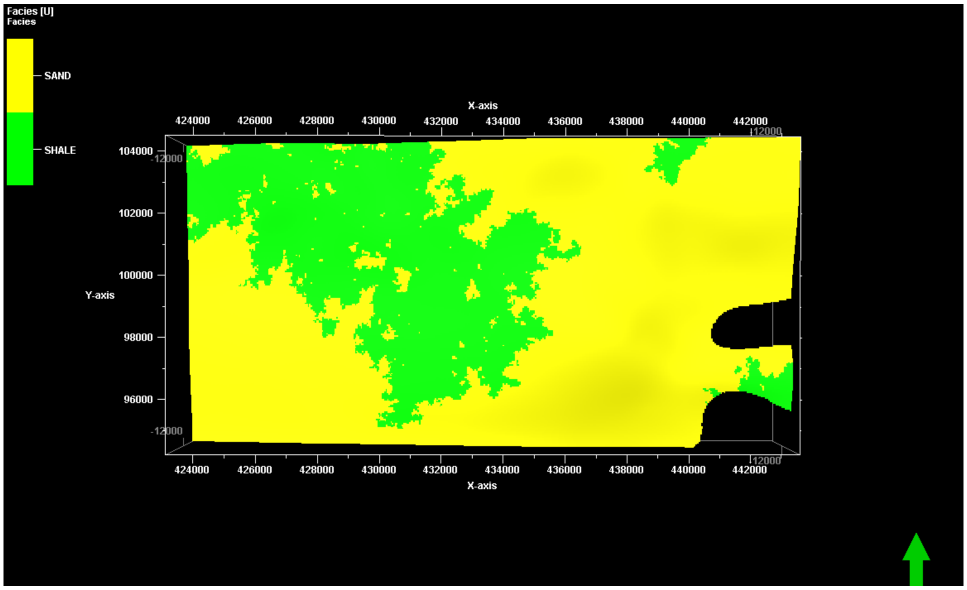

Fig. 6. Facies model of Reservoir 3

3.4 Net-to-gross model

The net-to-gross model was generated to differentiate the productive reservoir rock from the non-productive reservoir rock, sandstone being the principal reservoir rock of the field; the model was subsequently used as an input for volume calculation. Applying arithmetic-average upscaling and sequential Gaussian simulation, the net-to-gross of Reservoir 1 ranges from 0.5 to 3.5 with an average of 2.0, and that of Reservoir 3 ranges from 0.5 to 2.5 with an average of 1.5. The internal variability evident within each of these ranges, rather than a single uniform value per reservoir, is the expected outcome of the sequential Gaussian simulation of Equation 3, which draws each grid-cell value from a local distribution centered on the kriged estimate, so that plausible small-scale fluctuation is preserved instead of being smoothed away.

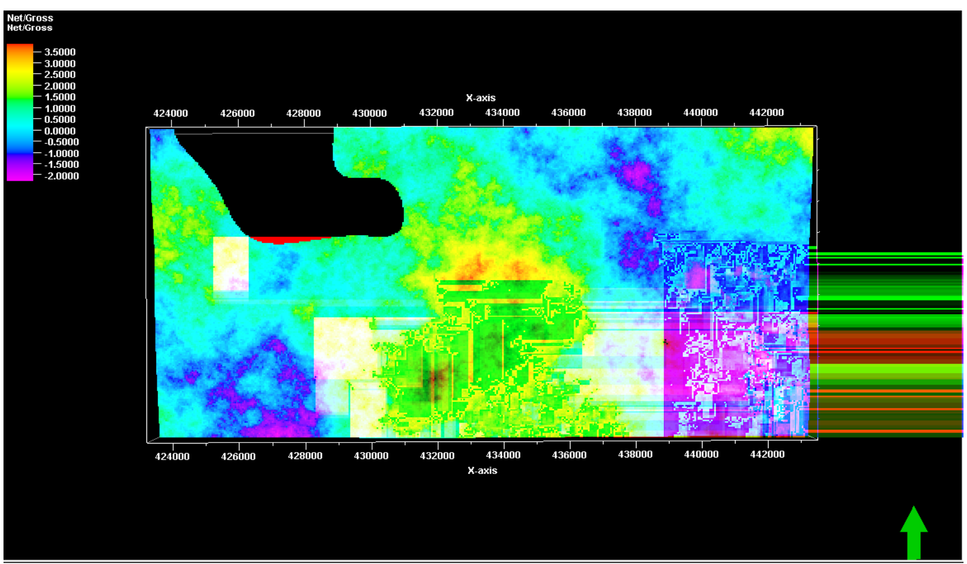

Fig. 7. Net-to-gross model of Reservoir 1

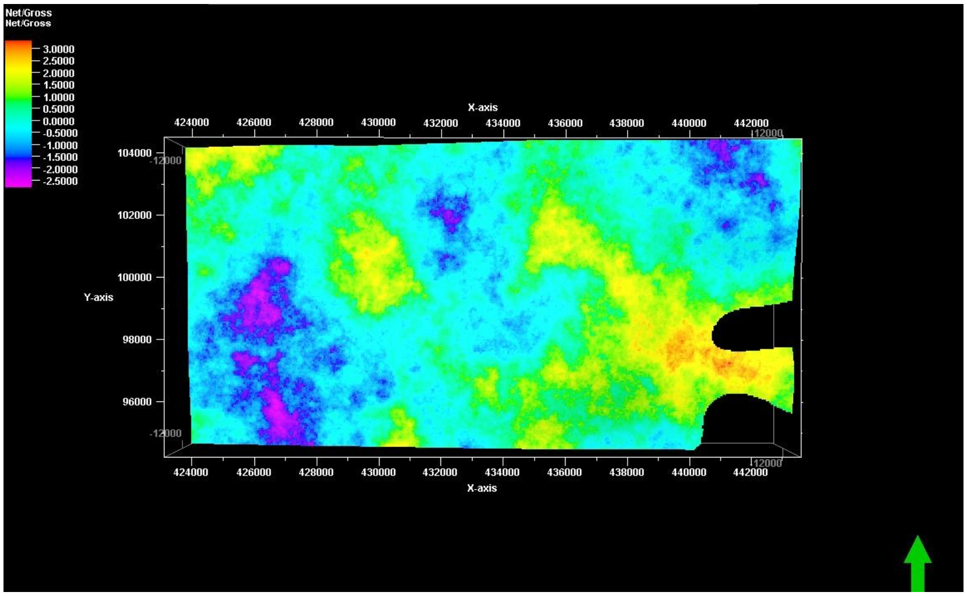

Fig. 8. Net-to-gross model of Reservoir 3

3.5 Effective porosity model

Since the quantity of oil in the reservoir is determined by its porosity, the porosity model was built on the petrophysical logs of the reservoirs, using arithmetic averaging to scale up the well logs and sequential Gaussian simulation to distribute porosity across the model. The model shows a porosity distribution of 19% to 28%, averaging 23%. The southeastern, southwestern and northwestern parts of Reservoir 1 show higher effective porosity than the northeastern part, whereas Reservoir 3 shows higher effective porosity in the south than in other parts of the reservoir. As with the net-to-gross model, this spatial pattern was generated by sequential Gaussian simulation conditioned to the facies model, so that porosity values away from well control were drawn from a local Gaussian distribution whose mean and variance are governed by the simple-kriging equations of Section 3.4.5, rather than assigned a single field-wide average.

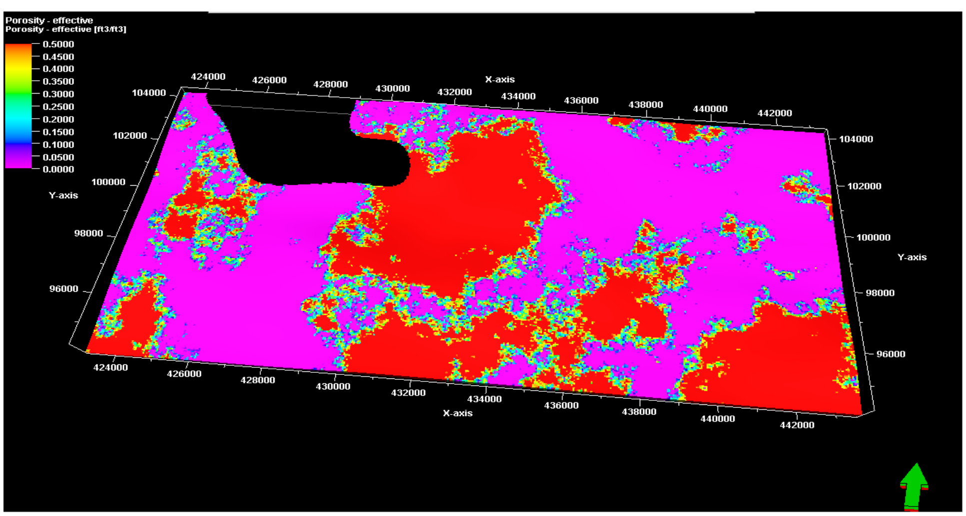

Fig. 9. Effective porosity model of Reservoir 1.

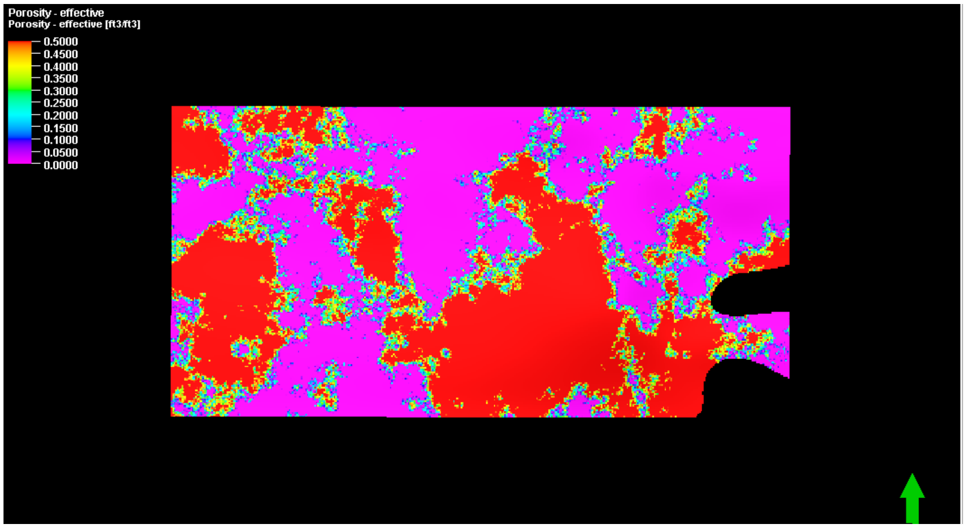

Fig. 10. Effective porosity model of Reservoir 3

3.6 Permeability model

Permeability, an integral reservoir parameter, determines the ease with which fluid flows through the pore space of the reservoir rock, as well as the orientation of the flow. The permeability model was constructed using the results of the permeability logs, applying harmonic averaging for upscaling and sequential Gaussian simulation for distribution across the grid. The model shows that Reservoir 1 has a higher permeability, averaging 222 mD, than Reservoir 3, while Reservoir 2 has little or no permeability. Because the permeability simulation was conditioned to the same facies model as porosity and net-to-gross, the mathematical formulation of Equation 3 ensured that the near-zero permeability of the shale facies was preserved as a distinct population from the higher permeability of the sand facies, rather than being blended into a single average value across the reservoir.

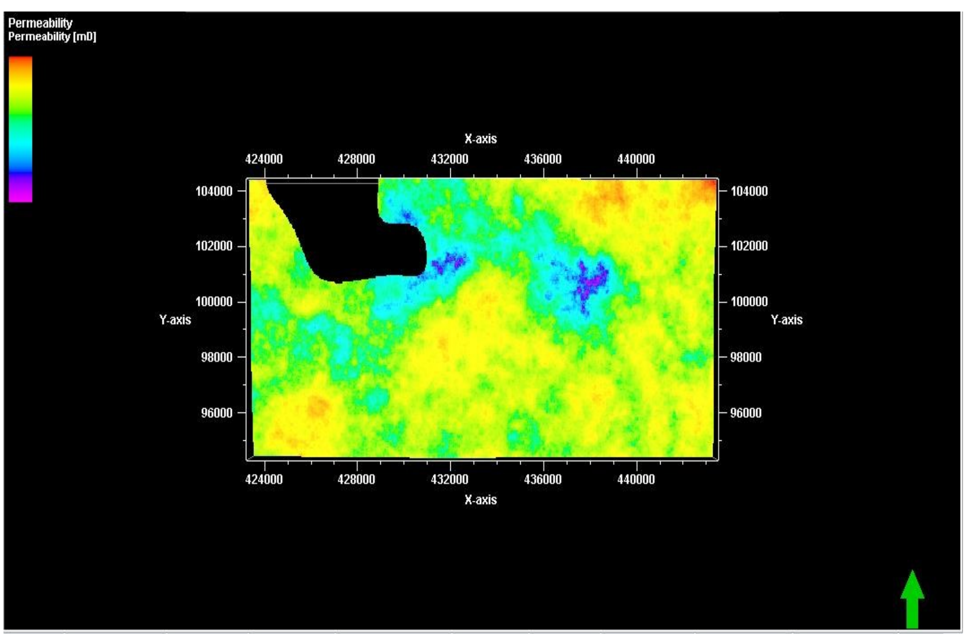

Fig. 11. Permeability model of Reservoir 1.

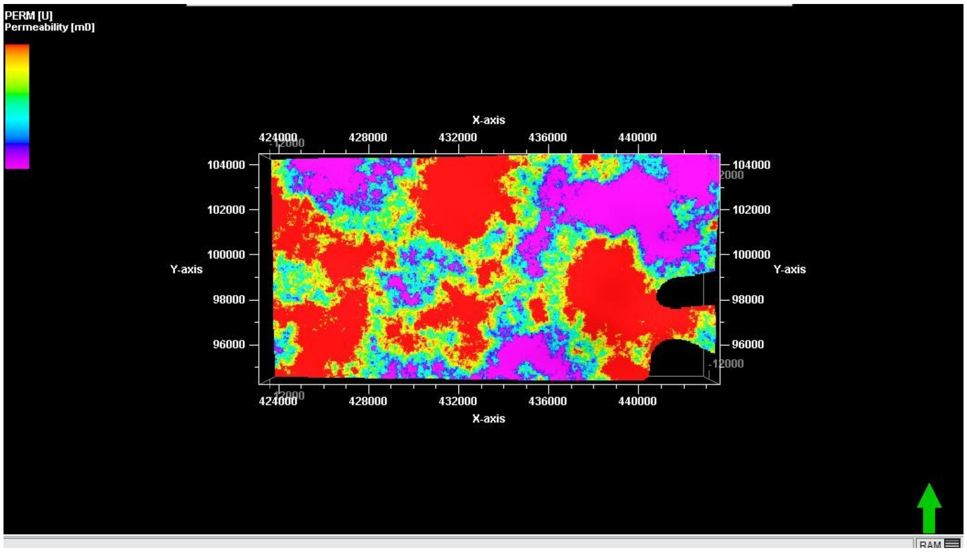

Fig. 12. Permeability model of Reservoir 3

3.7 Hydrocarbon saturation model

The hydrocarbon saturation model, representing the amount of pore spaces occupied by oil, gas and water is an important tool for delineating high-hydrocarbon habitats. Using the sequential Gaussian simulation method, the model shows that hydrocarbon saturation is highly concentrated in the northeastern–southwestern parts of Reservoir 1, and highly concentrated in the northwestern and northeastern parts of Reservoir 3, with minimal concentration in its southeastern part. These concentration patterns likewise reflect the kriging-based conditioning of Equation 3: hydrocarbon saturation values were simulated with the greatest confidence, and closest adherence to the well-log values, near the wells, with progressively more variability introduced by the simple-kriging variance term away from well control.

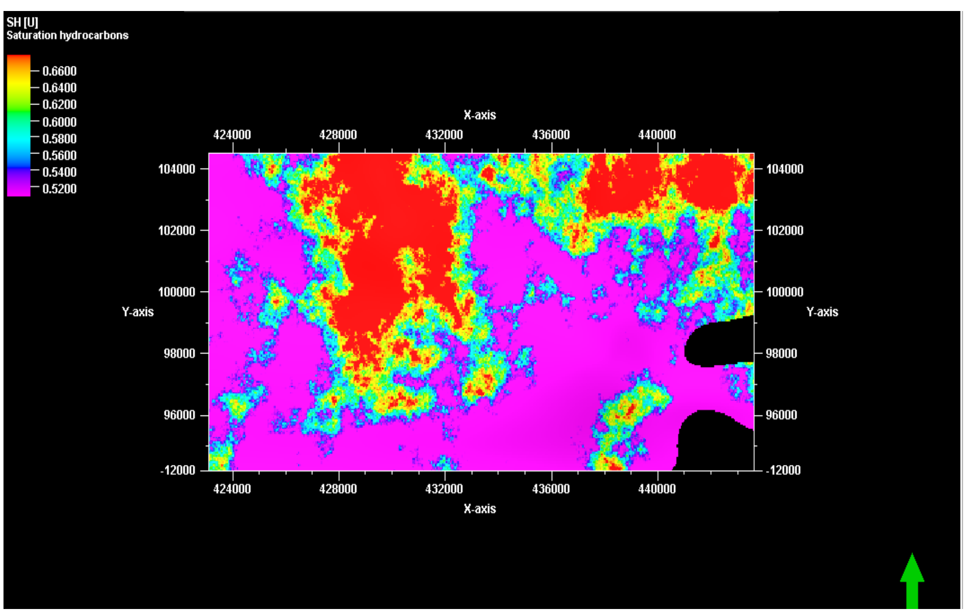

Fig. 13. Hydrocarbon saturation model of Reservoir 1

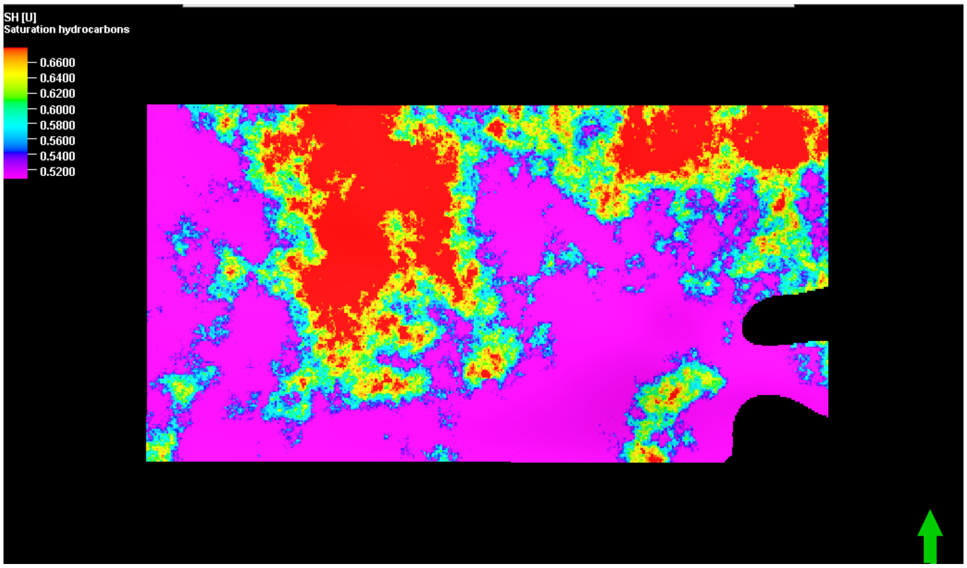

Fig. 14. Hydrocarbon saturation model of Reservoir 3

4.8 Summary of the petrophysical property models

Table 3 summarizes the ranges and averages of the key petrophysical properties returned by the static model across the three reservoirs.

4.9 Volumetric estimation

Reserve estimation used the structural and property models of each reservoir, together with the interpreted oil–water contact, in a Petrel model-based volumetric workflow to compute the Stock Tank Oil Initially in Place. The result reveals that Reservoirs 1, 2 and 3 have an oil in place of 6,090 × 10^3 bbl, 4,381 × 10^3 bbl and 5,658 × 10^3 bbl respectively. Reservoir 1 contains the largest hydrocarbon volume, followed by Reservoir 3, while Reservoir 2, despite exhibiting relatively high porosity, contains the smallest hydrocarbon volume owing to its comparatively limited net-to-gross and permeability. The ranking of reservoir prospectivity obtained from the static model agrees with the petrophysical evaluation, confirming that permeability and effective reservoir thickness exert a stronger influence on reserve potential than porosity alone. On this basis, Reservoirs 1 and 3 are commercially and economically more viable than Reservoir 2. Table 3 presents the full Petrel model-based volumetric breakdown, including gross rock volume (GRV), net volume, pore volume and hydrocarbon pore volume (HCPV), from which the STOIIP and recoverable-oil Fig.s were derived.

Table 2: Summary of the petrophysical property models of the study reservoirs

e	Range	Average
Effective porosity	19% – 28%	23%
Permeability	50 – 477 mD	222 mD (Reservoir 1)
Hydrocarbon saturation	56% – 66%	—
Net-to-gross	0.5–3.5 (R1); 0.5–2.5 (R3)	2.0 (R1); 1.5 (R3)

Table 3: Petrel model-based volumetric results for Reservoirs 1, 2 and 3

Reservoir	GRV (×10^6 ft^3)	Net volume (×10^6 ft^3)	Pore volume (×10^6 ft^3)	HCPV (×10^6 rb)	STOIIP (×10^3 bbl)	Recoverable oil (×10^3 bbl)
1	34,202	34,202	6,090	6,090	6,090	2,436
2	19,732	19,732	4,381	4,381	4,381	1,752
3	31,773	31,773	5,658	5,658	5,658	2,263

3.10 Discussion

The integrated static model demonstrates that the reservoir quality and hydrocarbon potential of the VAS Field are governed jointly by structural complexity and facies/petrophysical heterogeneity. The decrease in fault density with depth, captured in the structural model, is mirrored by a decrease in shale volume with depth in the facies model, so that the deeper Reservoirs 2 and 3 are structurally simpler and, in the case of Reservoir 3, of better net-to-gross and porosity than the shallower, more heavily faulted Reservoir 1. However, low permeability and a small net-to-gross, despite its structural simplicity, limit Reservoir 2 and explain its lower STOIIP relative to Reservoirs 1 and 3. This illustrates the value of building a fully integrated static model rather than relying on structural or petrophysical analysis in isolation, since the volumetric outcome of the field is controlled by the interaction of the structural framework, the facies distribution and the individually modeled petrophysical properties, and not by any one of these components alone.

Beyond explaining the spatial character of the individual property models, the variogram-based SIS–SGS mathematical framework of Section 3.4.5 has a direct bearing on the uncertainty attached to the STOIIP Fig.s of Table 3, because the simple-kriging variance grows with distance from the nearest well. The reservoir volumes reported here should be understood as most tightly constrained near wells KC1–KC3 and progressively less certain toward the flanks of Reservoirs 1–3, particularly in Reservoir 2, where fewer faults were mapped, net-to-gross and permeability, therefore, reveals that the reliability of the volumetric estimate are also lowest. The same stochastic approach that produced the single realization discussed above is, by construction, capable of producing multiple equiprobable realizations from the same variogram and conditioning data. Although only one realization was carried through to the volumetric estimate in this study, the mathematical basis for using additional realizations to place explicit confidence bounds on the STOOIP and recoverable-oil Fig.s, rather than reporting them as single deterministic numbers, is alre+ady established in the modeling workflow.

Placed alongside other recently published Niger Delta static models, the VAS Field results are modest in absolute volume but methodologically comparable in rigor. The combined oil in place of the three VAS reservoirs (16,129 × 10^3 bbl) is an order of magnitude smaller than that reported for the offshore KUKO Field, where Alakuko and Falowo (2023) computed total oil in place values of 642, 590 and 549 MMbbl for sands KUKO A, B and C respectively, and smaller again than the combined 164.6 MMbbl reported by Fajana, Olawale and Oyesomi (2025) for sands X, Y and Z of the Hamphidex Field, or the roughly 185 MMbbl reported by Etukudo *et al*. (2026) for a comparable structurally controlled eastern Niger Delta prospect. This difference is attributable chiefly to reservoir net-to-gross and permeability rather than to porosity: the effective porosity of 19–28% obtained for the VAS Field sits within, and in places above, the 16–25% range reported for Hamphidex and is close to the 22.8–26.1% range reported by Etukudo *et al*. (2026), while the average VAS permeability of 222 mD in Reservoir 1 is markedly lower than the 1,320–1,600 mD reported for the eastern Niger Delta prospect of Etukudo *et al*. (2026) and the 10–1,600 mD range at Hamphidex. The VAS Field is consequently better characterized as a smaller, more heterogeneous accumulation than as a poorly modeled one; the ranking of Reservoirs 1 and 3 as more prospective than Reservoir 2 (Section 4.9) reflects genuine differences in net-to-gross and permeability rather than any artifact of the modeling workflow.

Where the present study distinguishes itself from these comparator studies is in the explicit treatment of spatial uncertainty. The KUKO, Hamphidex and eastern Niger Delta studies cited above, like most Petrel-based static-modeling case studies published in the Niger Delta literature, report their SGS- and SIS-derived property models and volumetric outcomes as single deterministic realizations, without a formal accounting of how the kriging variance of Equation 3 varies across the field or of how that variance propagates into the reported STOIIP Fig.s. By setting out the full mathematical basis of the SIS–SGS workflow in Section 3.4.5 and relating it explicitly, in Sections 4.1 and 4.9, to the spatial reliability of the resulting facies, property and volumetric maps, the present study makes that uncertainty structure an explicit part of the reported result rather than an implicit property of the software used to generate it — a distinction consistent with the case Fajana (2023b) makes for treating reservoir-characterization uncertainty as a function of position relative to well control, and one that gives the VAS Field static model a stronger basis for risking its comparatively modest volumes than a single deterministic Fig. alone would provide.

4.0 Conclusion

The integrated static reservoir modelling of the VAS Field successfully characterized the structural framework, facies distribution, petrophysical properties and hydrocarbon volumes of the three investigated reservoirs. The structural model, comprising 31 interpreted faults, revealed a highly faulted reservoir system with fault occurrence decreasing with depth and major northeast–southwest-trending faults separating distinct structural blocks. The facies model indicated a progressive reduction in shale content with depth, suggesting comparatively better reservoir-quality conditions in Reservoirs 2 and 3 than in Reservoir 1.

The integrated petrophysical models showed effective porosity of 19–28%, permeability of 50–477 mD and hydrocarbon saturation of 56–66%, demonstrating appreciable spatial heterogeneity in reservoir quality. The combined structural, facies and petrophysical models provided a consistent geological framework for volumetric assessment and yielded STOIIP estimates of $6,090 \times 10^3$ bbl, $4,381 \times 10^3$ bbl and $5,658 \times 10^3$ bbl for Reservoirs 1, 2 and 3, respectively. Reservoir 1 therefore contains the largest estimated oil volume, followed by Reservoir 3, whereas Reservoir 2 contains the smallest volume. Although Reservoirs 1 and 3 exhibit more favourable geological and volumetric characteristics for further development evaluation, the static model alone does not establish commercial or economic viability.

Overall, the study demonstrates that integrating seismic interpretation, well-log-derived petrophysical properties, structural modelling, facies simulation and stochastic property modelling provides a more robust representation of reservoir heterogeneity than relying on isolated or deterministic interpretations. The resulting static earth model offers a sound geological basis for hydrocarbon volumetric assessment, uncertainty evaluation and subsequent dynamic simulation and field-development planning in structurally complex Niger Delta reservoirs.

5.0 References

Akinlabi, I. A., & Abiodun, A. O. (2024). Integration of seismic and well log data for reservoir characterization in offshore Niger Delta, Nigeria. *Journal of Geography, Environment and Earth Science International*, 28, 6, pp. 1–11.

Akintokewa, O. C., Fadiya, S. L., & Falebita, D. E. (2023). 3-D static modelling and reservoir quality assessment: A case study of FORT Field, Coastal Swamp Depobelt, Niger Delta. *Arabian Journal of Geosciences*, 16, 7, pp. 1–14. https://doi.org/10.1007/s12517-023-11471-5

Al-Mudhafar, W. J., Vo Thanh, H., Wood, D. A., & Min, B. (2024). Stochastic lithofacies and petrophysical property modeling for fast history matching in heterogeneous clastic reservoir applications. *Scientific Reports*, 14, pp. 279. https://doi.org/10.1038/s41598-023-50853-3

Archie, G. E. (1942). The electrical resistivity log as an aid in determining some reservoir characteristics. *Transactions of the AIME*, 146, 1, pp. 54–62.

Asquith, G., & Krygowski, D. (2004). *Basic well log analysis* (2nd ed.). AAPG Methods in Exploration Series, 16.

Coates, G., & Denoo, S. (1981). The producibility answer product. *The Technical Review*, 29, 2, pp. 44–144.

Cosentino, L. (2003). Integrated reservoir studies. *Bulletin of Canadian Petroleum Geology*, 51, 2, pp. 209–211. https://doi.org/10.2113/51.2.209

Doust, H., & Omatsola, E. (1989). Niger Delta. *American Association of Petroleum Geologists Bulletin*, 48, pp. 201–238.

Doust, H., & Omatsola, E. (1990). Niger Delta. In J. D. Edwards & P. A. Santogrossi (Eds.), *Divergent/passive margin basins* (AAPG Memoir 48, pp. 239–248). American Association of Petroleum Geologists.

Edem, P. A., Ugar, S. I., Edem, S. U., Obi, D. A., Mbange, C. E., & Obasi, M. E. (2026b). *Reservoir characterization and the quantitative assessment of hydrocarbon-bearing reservoir sands in the Otodi Field, Niger Delta*.

Emujakporue, G. O., & Ngwueke, M. I. (2013). Structural interpretation of seismic data from an XY Field, onshore Niger Delta, Nigeria. *Journal of Applied Sciences and Environmental Management*, 17, pp. 153–158.

Etukudo, N. J., Okpoji, A. U., Akpan, N. A., Aliyu, S. O., Anukam, B. N., Ndife, C. T., Okonkwo, P. C., Onuchukwu, E. E., Anumaka, C. C., Okafor, B. O., Otuuh, A. G., & Okpanachi, C. B. (2026). Integrated seismic attribute and petrophysical evaluation of structurally controlled hydrocarbon prospects in the eastern Niger Delta Basin, Nigeria. *International Journal of Research and Innovation in Applied Science*, 11, 4. https://doi.org/10.51584/IJRIAS.2026.110400023

Evamy, B. D., Haremboure, J., Kamerling, P., Knaap, W. A., Molloy, F. A., & Rowlands, P. H. (1978). Hydrocarbon habitat of tertiary Niger Delta. *AAPG Bulletin*, 62, pp. 1–39.

Fajana, A. O. (2020). 3-D static modelling of lateral heterogeneity using geostatistics and artificial neural network in reservoir characterisation of "P" Field, Niger Delta. *NRIAG Journal of Astronomy and Geophysics*, 9, 1, pp. 129–154. https://doi.org/10.1080/20909977.2020.1727674

Fajana, A. O. (2023). Hydrocarbon reservoir characterization methodologies and uncertainties as a function of spatial location: Review from gigascale to nanoscale. *FUOYE Journal of Pure and Applied Sciences*, 8, 2, pp. 82–99.

Fajana, A. O., Olawale, A. M., & Oyesomi, H. A. (2025). Quantitative reservoir evaluation and hydrocarbon volumetrics: An integrated petrophysical and 3-D static modeling approach in "Hamphidex" Field, Niger-Delta, Nigeria. *Journal of the Nigerian Society of Physical Sciences*, 7, 2, pp. 2429. https://doi.org/10.46481/jnsps.2025.2429

Hart, B. S. (2000). *3-D seismic interpretation: A primer for geologists*. SEPM (Society for Sedimentary Geology), Tulsa, pp. 129.

Hartman, D. J., & Beaumont, E. A. (1999). Predicting reservoir system quality and performance. In E. A. Beaumont & N. H. Foster (Eds.), *Exploring for oil and gas traps*. AAPG Treatise of Petroleum Geology.

Larionov, V. V. (1969). *Borehole radiometry*. Nedra.

Levorsen, A. H. (1967). *Geology of petroleum* (2nd ed.). Freeman, San Francisco, pp. 350.

Owolabi, O. O., Longjohn, T. F., & Ajienka, J. A. (1994). An empirical expression for permeability in unconsolidated sands of eastern Niger Delta. *Journal of Petroleum Geology*, 17, 1, pp. 111–116.

Poupon, A., & Leveaux, J. (1971). Evaluation of water saturations in shaly formations. *Proceedings of the SPWLA 12th Annual Logging Symposium*. Texas.

Rezaei, M., Emami Niri, M., Asghari, O., Talesh Hosseini, S., & Emery, X. (2023). Seismic data integration workflow in pluri-Gaussian simulation: Application to a heterogeneous carbonate reservoir in southwestern Iran. *Natural Resources Research*, 32, 3, pp. 1147–1175. https://doi.org/10.1007/s11053-023-10198-0

Schlumberger. (1974). *Log interpretation manual/charts*. Schlumberger Well Services.

Simandoux, P. (1963). Dielectric measurements in porous media and application to shaly formation. *Revue de l'Institut Français du Pétrole*, 18, Supplementary Issue, pp. 193–215.

Sonny, T., Oluwafisayo, M., Ebere, B., Tolulope, A., & Fisayo, I. (2024). Reservoir heterogeneity and boundary delineation using numerical well test analysis and multi-seismic attributes in complex channel environment. *SPE Nigeria Annual International Conference and Exhibition*, Lagos, Nigeria. https://doi.org/10.2118/221782-MS

Wyllie, M. J. R., & Rose, W. D. (1950). Some theoretical considerations related to quantitative evaluation of the physical characteristics of reservoir rock from electric log data. *Journal of Petroleum Technology*, 2, 4, pp. 105–118.

Declaration:

Consent for publication

Not Applicable

Data Availability Statement:

The datasets supporting the findings of this study are available in the manuscripts

Conflict of Interest

Not Applicable

Ethical Considerations

Not applicable

Funding

The author(s) declared no source of funding

Authors' Contributions

Philip Asuquo Edem conceived the study, performed the seismic and well-log interpretation, constructed the structural, stratigraphic, facies and petrophysical models, conducted the volumetric analysis, interpreted the results, and prepared the manuscript. Selong Unanaonwi Edem contributed to study supervision, methodological review, data interpretation, validation of the reservoir model and results, critical revision, and final approval of the manuscript.